Enhancing the Reliability of Resting ECGs via Deep Learning–Driven Motion Artifact Detection

August 25, 2025

S.A. Nanayakkara, R.G.N. Meegama*

1 Affiliation Department of Computer Science, Faculty of Applied Sciences, University of Sri Jayewardenepura, Gangodawila, Nugegoda, Sri Lanka.

‡

¶

* Corresponding author: rgn@sjp.ac.lk

Abstract

This study presents a novel two-stage framework to enhance the reliability of resting electrocardiogram (ECG) signals by addressing motion artifacts that often compromise diagnostic accuracy. In the first stage, motion artifacts are mitigated using stationary wavelet transform coupled with Savitzky-Golay filtering, effectively preserving critical ECG morphological features such as the QRS complex. The second stage employs a deep convolutional neural network to classify ECG signals as either usable or artifact-corrupted, achieving a classification accuracy of 98.76%. Utilizing a 12-lead ECG dataset from PhysioNet, the proposed unified CNN model outperforms individual lead-specific models, offering superior computational efficiency (1.6 seconds vs. 21.7 seconds for predictions) and reduced storage requirements (1 GB vs. 15 GB). The approach demonstrates high sensitivity (98.74%) and specificity (98.77%), ensuring robust detection of noisy signals. By integrating advanced preprocessing with deep learning, this framework enhances ECG signal clarity, reducing the risk of misdiagnosis in clinical settings. Future work will focus on real-time integration into ECG devices, expanding datasets to include diverse cardiac pathologies, and incorporating multimodal signals to further improve artifact detection, paving the way for automated, reliable ECG diagnostics.

Author summary

Introduction

The ECG is a vital tool for diagnosing various heart abnormalities [1]. By placing electrodes on specific locations on the skin, ECG measures the electrical activity

associated with the heart muscle, which is propagated through various tissues to the skin's surface. The resulting ECG waveform, consisting of P-wave, QRS-complex and T-wave, provides valuable information about the heart's function, enabling medical professionals to detect potential issues [2].

The cardiac conduction system, which includes the sinoatrial (SA) node and atrioventricular (AV) node, plays a crucial role in maintaining the heart's rhythm and the proper function [3, 4]. However, despite the potential of ECG to identify heart diseases, a clear and uninterrupted signal is necessary for accurate diagnosis. Motion artifacts, which result from involuntary muscle movements and skin stretching, can distort ECG signals and complicate interpretation [5, 6].

Researchers have long sought effective methods to reduce motion artifacts and extract clean ECG signals. Traditional mathematical models and standalone machine learning approaches have struggled to achieve satisfactory results due to the low Signal-to-Noise Ratio (SNR) in ECGs. Moreover, interpreting ECG data requires expertise, further limiting the applicability of these methods.

There are various types of ECGs, categorized based on the method of acquisition and the purpose of the test. These include resting ECG, exercise stress test (EST), ambulatory ECG (Holter monitoring) and event monitoring. Resting ECG, as the name implies, is performed while the patient is at rest, typically lying down. This type of ECG is commonly used as the first step in diagnosing heart diseases and assessing the heart's overall function.

Resting ECG is selected for this study because of its widespread clinical use and vulnerability to motion artifacts, even when patients are at rest. As noted earlier, involuntary muscle activity and skin stretching can introduce noise into the ECG signal during rest. These artifacts may cause misdiagnosis or necessitate further testing, leading to inconvenience for both patients and healthcare providers. This study aims to improve the diagnostic accuracy of resting ECG by employing deep learning techniques to remove motion artifacts, thereby demonstrating enhanced signal usability.

Recent advances in deep learning and neural networks have shown promise in addressing these challenges. By employing deep convolutional neural networks (CNN), it is possible to automate motion artifact removal in resting ECG signals and generate cleaner outputs for medical professionals to analyze. This study aims to develop a novel deep learning-based approach for motion artifact removal in resting ECG signals and verify its effectiveness by comparing it with existing methods.

1 Related Work

The challenge of motion artifact removal in ECG signals has been addressed through multiple signal processing and machine learning approaches. Early adaptive filtering methods [7] utilized custom motion sensors as reference inputs but demonstrated limited effectiveness for low-frequency noise components. Subsequent work employed Empirical Mode Decomposition (EMD) for real-time artifact detection in ambulatory monitoring systems [8], though without providing robust removal capabilities.

Wavelet-based techniques have shown particular promise, with Stationary Wavelet Transform (SWT) proving effective for artifact suppression while preserving QRS complex morphology [9]. Comparative studies have demonstrated SWT's superiority over conventional Discrete Wavelet Transform (DWT) for ECG de-noising applications [10]. Independent Component Analysis (ICA) approaches [11] achieved noise separation but struggled with motion artifact specificity, particularly in 12-lead configurations.

Recent advances in deep learning have revolutionized ECG analysis. Personalized 1D CNNs have been developed for patient-specific ECG classification [12], while hybrid

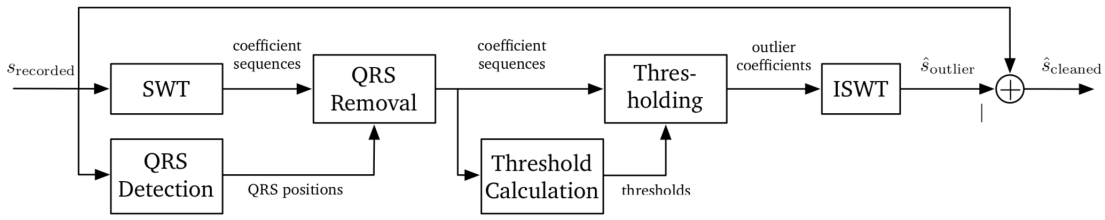

Fig 1. Schematic diagram of the multi-resolution thresholding algorithm [9].

architectures combining wavelet transforms with neural networks have shown improved denoising performance [13]. Template-based adaptive filtering methods [14] and comprehensive noise removal frameworks [15] have further advanced the field. Two-stage processing pipelines integrating wavelet de-noising with machine learning classifiers [16] have demonstrated particular effectiveness. Deep learning approaches for automated ECG quality assessment [17] have achieved state-of-the-art results, though computational complexity remains a concern for real-time implementations. The current work builds upon these foundations while addressing key limitations in artifact removal completeness and computational efficiency.

Materials and methods

1.1 Data Preparation and Collection

When a resting ECG is taken, an encrypted data file is created that comprises all lead information as well as important raw data. While a normal ECG setup includes a mechanism to convert such data to ASCII format, retrieving and interpreting such data is entirely dependent on the device manufacturer. As such, we considered the publicly accessible *PhysioNet* database [18] containing a 12-lead resting ECG. Prior knowledge included in these corpus enabled us to design proposed approaches capable of achieving the desired results in a laboratory context.

1.1.1 Data Pre-processing

Surface measurements of the human body always contain a variety of noise that must be filtered out [15] before attempting to process the data using any pipelined technique. Baseline wandering is a term that refers to a sort of slow frequency noise in the ECG signal that results in a fluctuating baseline. The primary cause of wandering is the impedance between the ECG leads and the patient's skin, which changes as the chest moves slightly while breathing, altering the distance between the heart and the leads. Although, baseline wandering may result in an incorrect ECG interpretations, such abnormalities can be estimated and removed [19, 20]. While these methods effectively address baseline wandering, they demonstrate limited efficacy in suppressing persistent motion and muscle artifacts.

1.2 Removal of Motion Artifacts

Visual interpretation of an ECG is challenging because motion artifacts are often mixed with raw ECG data to create an output that obscures each heartbeat [21]. We will cover implementation specifics, tools utilized and the mathematical foundations for motion artifact reduction in the following sections.

1.2.1 Methodology Selection

Because the primary objective of this research is to automate the removal of motion artifacts and to assess the processed signal using a machine learning model, the feasibility of implementing each technique is critical for reaching acceptable results. As in Section 1, the bulk of prior work is related to hardware implementations. In comparison, we offer a software solution that makes use of machine learning techniques to accomplish the primary goal.

1.2.2 Implementation

It must be noted that only lead I data is considered in this section for the sake of explanation and clarity. We calculate the outlier $\hat{s}_{\text{outliers}}$ and obtain a cleaned signal using Eq. 1, $n \in [1, N]$ where N is the number of ECG samples as

$$\hat{s}_{\text{cleaned}}(n) = \hat{s}_{\text{recorded}}(n) - \hat{s}_{\text{outliers}}(n) \tag{1}$$

Calculating the amount of noise present in the signal is possible and can be used to obtain a cleaned ECG because when two signals overlap, the artifacts and signals are added up to produce the result by using SWT coefficient sequence and multi-resolution thresholding, as depicted in Fig. 1.
Consider the role of DWT [22]. It decomposes a signal into a collection of mutually orthogonal wavelet functions which are dilated, translated and scaled copies of a common wavelet termed as a "mother wavelet". Each DWT has two filters referred to as the *filter-bank* [22] which calculates the coefficients of a discrete collection of child wavelets for a given mother wavelet. Because DWT is applicable to non-stationary signals and the ECG meets this criterion, this technique becomes a well-established method for ECG de-noising and is capable of decomposing the signal to correct the relevant frequency spectrum. However, one of DWT's primary disadvantages is its lack of translation invariancy. Assume there is a signal X and, even with a periodic signal extension, the DWT of a translated version of X is not, in general, the translated version of the DWT of X. This demonstrates the need of using SWT, which compensates for DWT's lack of translation invariance by averaging a slightly modified DWT termed ε-decimated DWT.
The main two reasons for the selection of SWT [23] in this proposed work are as follows:

- SWT removes the translation-variance of the DWT because SWT is invariant against translations of the signal in the time domain [24].
- As the decimation of the coefficients at each level of the transformation is omitted, more samples in the coefficient sequences are available to detect possible outliers [9].

Implementing SWT is based on the method proposed in [25]. As depicted in Fig. 2, SWT generates two sequences, a wavelet coefficient and a scaling coefficient denoted by $\{w_1, w_2, ..., w_M\}$ and $\{d_1, d_2, ..., d_M\}$, respectively where M is the decomposition level of the SWT and d_0 is the input signal. In this implementation, the very first M has to be calculated.

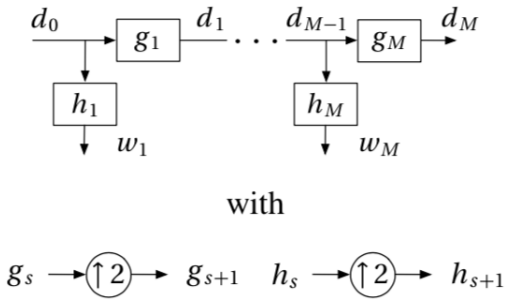

Fig 2. Implementation of SWT where h_s and g_s denote responses of low pass and high pass filters, respectively. The operator $\uparrow$ denotes the decimator with a factor of 2 [25,26].

De-noising an ECG signal involves several steps starting from SWT using the Haar as the mother wavelet as shown in Fig. 1. At each step, the relevant normalized median absolute deviation is used to compute a threshold. Finally, the threshold signals are converted back to ECG using an inverse SWT function. After de-noising the ECG [27], we proceed to identify the QRS complexes. For this purpose, the de-noised signal is subjected to a high pass filter to remove low frequency signals as shown in Fig. 3 [28].

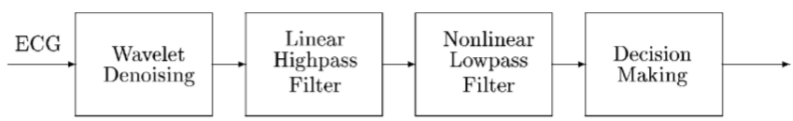

Fig 3. QRS detection pipeline [28].

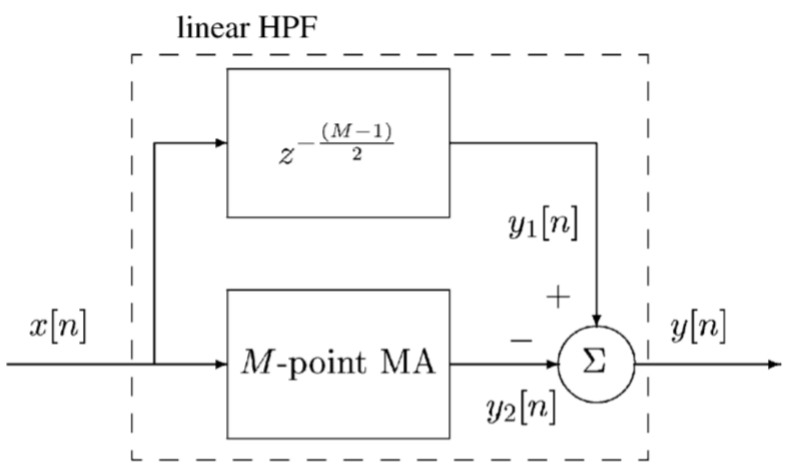

Fig 4. Architecture of HPF [28].

According to Fig. 4, initially, the de-noised signal passes through an M-point moving-averaged linear high pass filter to accentuate the QRS complex. This filter with an ideal delayed system is used at this point as it causes the input function to shift forward in the time domain. The filtering process is followed by subtracting the result from the delayed input samples, point wise, to produce a high pass filter (HPF) having a finite impulse response (FIR). Let us consider N number of ECG samples where $n \in [1, N]$. Then, the output $y_1[n]$ and the delayed sample $y_2[n]$ are calculated as

$$y_1[n] = \frac{1}{M}\sum_{m=0}^{M-1} x[n-m] \tag{2}$$

$$y_2[n] = x[n - \frac{(M-1)}{2}] \tag{3}$$

where $x[n]$ represents the de-noised ECG input data and M is the filter length. If M is too large, P or T waves will be adversely enhanced [28]. As such, for convenience, M is restricted to an odd value heuristically initialized to 5. The output of the high pass filter is calculated as

$$y[n] = y_1[n] - y_2[n] \tag{4}$$

The next phase of the QRS detection mechanism is to send the output of the HPF into a non-linear low pass filter (LPF). This filtering technique is constructed using a cascade of point-by-point squaring operation having a moving window integration [28]. If K denotes the summation interval (or window length), the QRS feature $z[n]$ is given as

$$z[n] = \sum_{k=1}^{K-1} y^2[n-k] \tag{5}$$

Because the threshold proposed by Chen et al. [9] is not robust against motion induced artifacts, a new threshold T_{QRS} is expressed as

$$T_{QRS} = \hat{\mu}_(maxima) - c \cdot \hat{\sigma}_(maxima) \tag{6}$$

where $(\hat{\mu})$ and $(\hat{\sigma})$ denote strong estimates of the mean and scale, respectively. Also the value for c has to be selected carefully because it depends on prior amount of impulsive noise in the data. The constant c should be chosen greater or equal to 2 to ensure detection of all QRS complexes and it depends on the prior knowledge of the amount of impulsive noise present in the data. In case impulsive noise is not included in the data, c is kept at above 2.5. However, as noise is inevitable in raw ECG, it is advisable to maintain $c \in [2, 2.5]$. As we have evaluated T_{QRS} from Eq. 6, the detected QRS, $QRS_{Detection}$ is calculated as

$$QRSDetection = \begin{cases} QRScomplex & \text{if } z[n] \leq T_{QRS} \\ None & \text{otherwise} \end{cases} \tag{7}$$

where $QRS_{complex}$ gives a valid QRS signal.
Prior to the last step in motion artifact reduction, a thresholding must be done following the sequence of processes as described above. To begin with, the lower and higher threshold sizes are determined using the SWT findings while the number of ECG data points and sequences for thresholding (SWT outputs) must be recorded. Subsequently, the upper and lower thresholds for each sequence are computed.
For this purpose, maxima and minima of estimated median $(\hat{\mu})$ and scale $(\hat{\sigma})$ is used to calculate the least upper bound (c_{max}) and the least lower bound (c_{min}) as

$$c_{max} = \hat{\mu}_(maxima) + \hat{\sigma}_(maxima) \tag{8}$$

$$c_{min} = \hat{\mu}_(minima) - \hat{\sigma}_(minima) \tag{9}$$

where $\hat{\mu}_(maxima)$ and $\hat{\sigma}_(maxima)$ denote the maxima of the estimated median and scale, respectively. Also, $\hat{\mu}_(minima)$ and $\hat{\sigma}_(minima)$ give the minima of estimated median and the scale, respectively. The upper threshold, T_u, is then calculated as

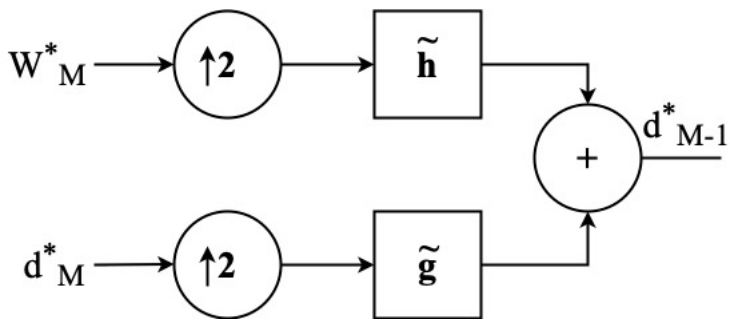

Fig 5. Steps of the Inverse Stationary Wavelet Transform (ISWT).

$$T_u = \begin{cases} c_{max} & \text{if } empty(Array_{Max} > c_{max}) \\ \hat{c}_{max} & \text{otherwise} \end{cases} \tag{10}$$

where $Array_{Max}$ is the array containing the maximum value of each sequence and

$$\hat{c}_{max} = max(Array_{Max} < c_{max}) \tag{11}$$

The lower threshold, T_l, is obtained by

$$T_l = \begin{cases} c_{min} & \text{if } empty(Array_{Min} < c_{min}) \\ \hat{c}_{min} & \text{otherwise} \end{cases} \tag{12}$$

where $Array_{Min}$ is the array containing the minimum value of each sequence and

$$\hat{c}_{min} = min(Array_{Min} > c_{min}) \tag{13}$$

Subsequently, new wavelet coefficient sequences ($w_s^*(n)$) and scale coefficient sequences ($d_M^*(n)$) are calculated as

$$w_s^*(n) = \begin{cases} w_s(n), & \text{if } d_s(n) > T_{s,u} \\ w_s(n), & \text{if } d_s(n) < T_{s,l} \\ 0, & \text{otherwise} \end{cases} \tag{14}$$

$$d_M^*(n) = \begin{cases} d_M(n), & \text{if } d_M(n) > T_{M,u} \\ d_M(n), & \text{if } d_M(n) < T_{M,l} \\ 0, & \text{otherwise} \end{cases} \tag{15}$$

where $d_s(n)$ and $T_{s,u}$ are the scale coefficient and upper threshold of level s, respectively while $T_{s,l}$ gives the lower threshold of level s. Also, $T_{M,u}$ and $T_{M,l}$ denote the upper and lower thresholds of level M.
The method shown in Fig. 5 produces a perfect reconstruction of the signal, where $\tilde{\mathbf{g}}$ gives the inverse scaling filter coefficients and $\tilde{\mathbf{h}}$ is the inverse wavelet filter coefficients.

1.3 Deep ConvNet for ECG Evaluation

The 2nd step of this study includes the implementation of a deep CNN to determine whether artifact-free ECG signals can be utilized for diagnostic purposes. Clinicians often identify any ECG abnormality using their professional knowledge accumulated throughout the years. Yet, a clinician may need to examine each wave in the stream in order to get a useful visual representation of the signal.

We utilized machine learning techniques to interpret ECG signals and compare the findings with ground truth acquired from an expert in order to verify whether the program will be able make predictions accurately and such predictions must be generated quickly.

1.3.1 Data Preparation

Selecting an appropriate architecture and amassing relevant data for training, evaluation and testing are often difficult challenges when deploying CNNs. This section will discuss the methods used to gather and prepare data for this purpose.
As this study examines all 12 ECG leads, each lead may be assessed individually. Due to the fact that an ECG repeats the same signal (although not identical) at each beat and just a few seconds of the ECG are used for resting diagnosis, the size of each signal may be further reduced. Over 3000 image having a resolution of 74 x 448 pixels each are produced and saved in this experiment depending on the relevant leads.
Additionally, to simplify training and testing, the data is randomly mixed via TensorFlow before feeding into the CNN. Each lead had three folders containing testing, training and validation data that are randomly split using the $80\% - 20\%$ separation method (80% for training and the remainder for validation).

1.3.2 Architecture

It is standard practice in the research community to use a pre-trained ConvNet model using millions of images classified into thousands of categories and to utilize it as a feature extractor or weight initializer for a particular job [29]. Finding a suitable network that is pre-trained for the area of interest, on the other hand, is challenging. The most difficult part of developing an architecture from scratch is assessment of performance heuristically which consumes a significant amount of both human and physical resources. Thus, transfer learning is used in a specific portion of this study and will be addressed in more detail later.
As we are unable to locate a pre-trained ConvNet in the ECG domain, an already-tuned network is modified as a significant quantity of data with augmentation is already available to train such a network. We utilized a simplified version of VGGNet [30] to detect noise in the ECG as such architectural modifications have been used in the literature to improve the accuracy in a variety of deep learning applications [31, 32]. This model comprises of four weight layers separated by *Sigmoid* and *Maxpooling* layers. In the final layer, the *Sigmoid* activation function is used to maximize the binary classification outcome.

1.3.3 Model Implementation

All model parameters, such as the batch size, number of epochs, etc., must be provided during model implementation. Table 1 indicates the number of images are collected for each lead. To produce a significant number of data for training, testing and validation, the images are enhanced using the Keras Image augmentation package. In addition, this library applies modifications with randomly chosen parameters within the given range to all the original pictures in the training set, guaranteeing that identical images are never generated at each learning epoch..
Moreover, the images had to be padded to make them square because the originals are of the size 74 x 448 pixels. Recent work has shown that padding images to create square shapes provide more accurate results than non-padded image data sets during training, testing and validation [30, 33, 34].

Another crucial fact to note is that the model may not be trained properly owing to variations in pixel intensities between training, validating and testing images. To resolve this issue, it is essential to treat all of these images uniformly. This crucial step is handled by *Rescale*, which configures the image rescaling factor where if 0 is given for *Rescale*, no rescaling occurs. However, when a valid scale is specified, the intensity value of each pixel in the image is multiplied by that scale prior to any image alteration to ascertain that the contribution of each image is identical and also to utilize the average pace of learning that we indicate.

Table 1. Actual number of images used based on leads and categories.

Leads	Number of images	
	with noise	without noise
I	1565	1565
II	1565	1565
III	1565	1565
aVR	1565	1565
aVF	1565	1565
aVL	1565	1565
V1	1565	1565
V2	1565	1565
V3	1565	1565
V4	1565	1565
V5	1565	1565
V6	1565	1565

As previously mentioned, some images include pixels with a high pixel density while others have pixels with a low pixel density. Without a scaling function, the model continues to use all such images with weights and learning rate. This is a major drawback and we will have an effect on its accuracy because when black and white data are evaluated, images with a higher white pixel count contribute more to the total loss than images with a lower white pixel count. However, back propagation will account for all such values lost without any preference to a particular image. Also, as a cleaned ECG has a higher percentage of white pixels, this tendency has the practical effect of decreasing the accuracy in binary classification. However, this effect may be significantly reduced by minimizing the contribution of white color.

1.3.4 Training

Prior to the training step, we must select a suitable model for ECG assessment. This can be accomplished by using several models to evaluate the 12 leads or by using a single model to evaluate all 12 leads. Using several models for the evaluation is attempted by assigning the first model to *Lead I* according to the selected architecture for the training after augmenting $3,000$ images to $23,500$. This process is continued by augmentation $15,000$, $8,500$ and $3,750$ images for training, testing and validation, respectively. After training a single model, the researcher utilizes transfer learning to create appropriate models for the other 11 leads using Keras and the previously trained model's HDF5 data. The disadvantage of employing multiple models is that several models are required to detect motion artifacts in all 12 leads. However, resource allocation may be reduced significantly if a single model is employed to detect such artifacts in all 12 leads. To do this, the data from the 12 leads is divided into two categories: with and without noise. Following that, the $36,000$ pictures are increased to $47,000$ and divided into $30,000$, $17,000$ and $7,500$ images for training, testing and validation, respectively.

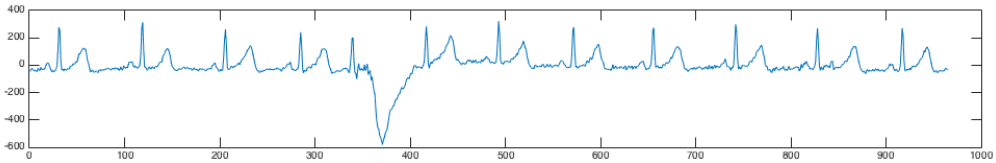

Fig 6. The ECG generated by data augmentation methods similar to ECG used in [9]

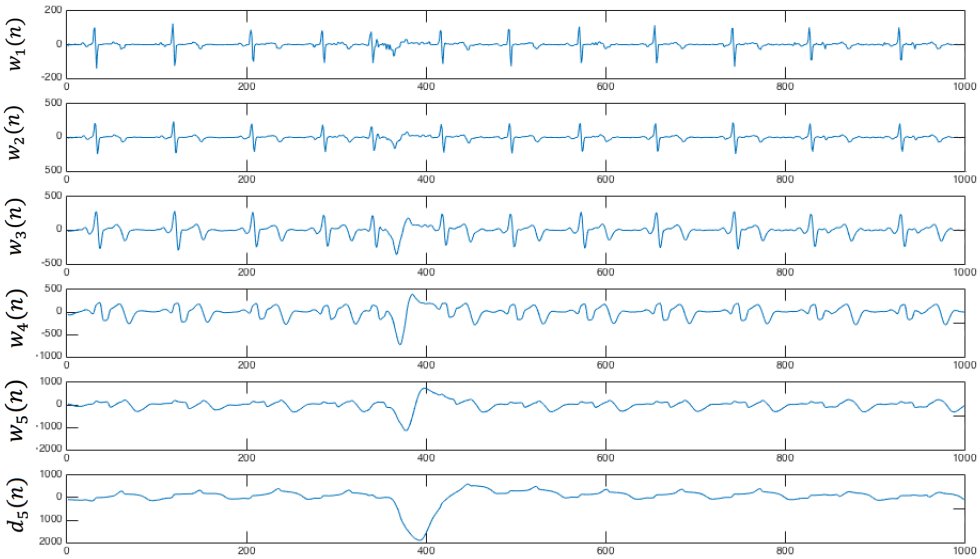

Fig 7. Decomposition levels after applying SWT on the ECG.

Results & Discussion

1.4 Motion Artifacts Removal

The results of a single lead (Lead I) ECG data are presented in this section for the sake of illustration.

Fig. 6 illustrates an ECG that is generated for validation purposes and has obvious motion artifacts, most notably, around the fourth heart beat. As a consequence, this may be used to determine if the chosen method performs as anticipated.

As shown in Fig. 7, each level of the SWT is detected and utilized to eliminate relevant noise components from the original signal using five wavelet coefficients. This enables us to prevent QRS detection by highlighting outliers that can be eliminated.

Fig. 8 depicts the thresholds of the ECG obtained to calculate the error. To distinguish outliers from the actual ECG signal, we compute an upper and lower thresholds for each coefficient sequence by dividing each into segments and subsequently, the maxima and minima for each is computed using Eqs. (8, 9).

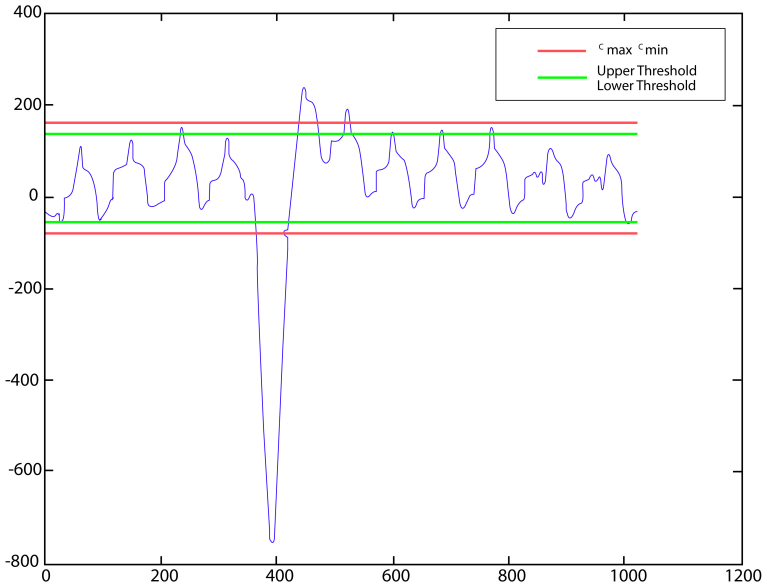

Fig 8. Thresholds with bounds.

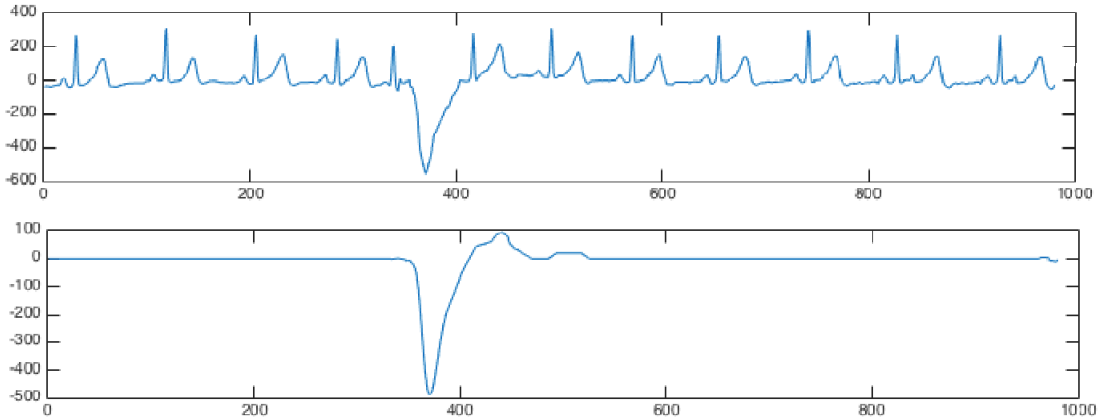

Fig 9. (top) ECG obtained and (bottom) ECG error.

Fig. 9 clearly shows the error calculated from raw ECG data. Although this error is deducted from raw data to produce a corrected ECG, the it may not exhibit 100% accuracy. To address this issue, *Savitzky-Golay filter* [35] is introduced to improve the signal clarity while preserving the accuracy.

Fig.10 shows the effect of filtering ECG signals where we analyzed 500 unprocessed 1000Hz-generated ECGs from healthy and unhealthy subjects which produced an MSE = 0.0014 with filtering and MSE = 0.0018, without filtering. Moreover, we set M = 7 in this interpretation as it produced the lowest MSE Table 2. Fig 11 presents the processed ECG signal following motion artifact removal and smoothing, demonstrating improved signal quality.

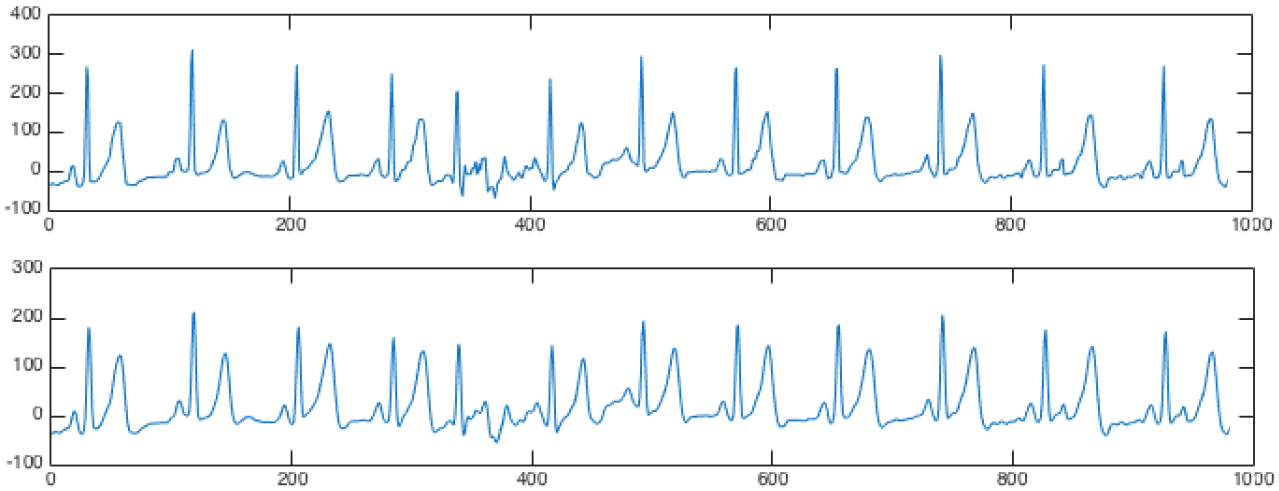

Fig 10. ECG signals (top) without filtration and (bottom) with filtration.

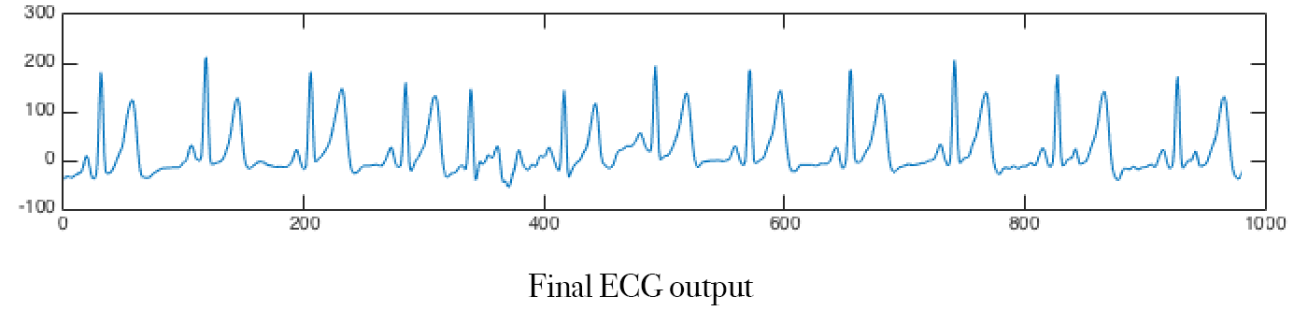

Fig 11. Final lead I ECG after removing motion artifacts and improving details with Savitzky-Golay filter.

Table 2. MSE values against M (decomposition level).

M value	MSE
1	0.0212
2	0.0050
3	0.0081
4	0.0102
5	0.0031
6	0.0021
7	0.0014
8	0.0018
9	0.0022
10	0.0029

1.5 Deep ConvNet for ECG Evaluation

This section explains all intermediate and the final outputs of ConvNet training.

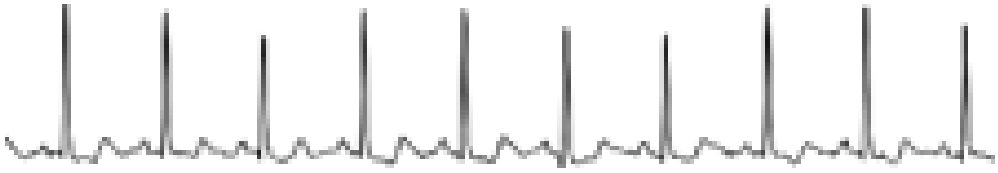

Fig 12. Sample lead I ECG image used to train models (Without noise).

1.5.1 Data Preparation

Data preparation is one of the most time-consuming activities in this stage because a huge data collection is required to commence the task. A single ECG signal may not usually provide sufficient information to remove noise components due to rapid movements of the subject resulting in noise together with increased heart rate. Thus, an ECG with two or five beats is insufficient to detect the presence of significant noise when the time laps is short. To avoid this barrier, we created a method for capturing pictures in an ECG with ten to fifteen beats as seen in Fig. 12.

1.5.2 Models Evaluation

Determining the optimal number of convolutional neural networks (ConvNets) required to achieve high classification accuracy presents significant computational challenges. We address this through two distinct approaches: (1) training individual models for each of the 12 ECG leads and (2) developing a unified model encompassing all leads. To optimize input processing, we systematically evaluated image padding techniques by comparing model performance with and without padding. Our experiments demonstrated superior accuracy for padded inputs (98-99%) compared to unpadded alternatives (95.8-96%), establishing padding as the preferred preprocessing method for the final architecture.
The Table 3 shows the training accuracy of each model trained to evaluate relevant lead data.

Table 3. Performance of trained models.

Model (Lead specific)	True Positive	True Negative	False Positive	False Negative	Training Accuracy
I	315	309	9	3	98.11%
II	288	318	3	32	94.53%
III	315	314	4	5	98.59%
aVR	314	320	0	6	99.06%
aVF	313	315	5	6	98.12%
aVL	309	316	4	11	97.65%
V1	314	315	5	6	98.28%
V2	314	318	2	6	98.75%
V3	290	319	1	30	95.15%
V4	309	316	4	11	97.66%
V5	315	316	4	5	98.59%
V6	297	318	2	23	96.09%

After training the single model to assess data taken from the 12 leads, we achieved an overall accuracy of 98 percent. However, for each individual lead, Table 4 indicates the degree to which this assessment is correct.

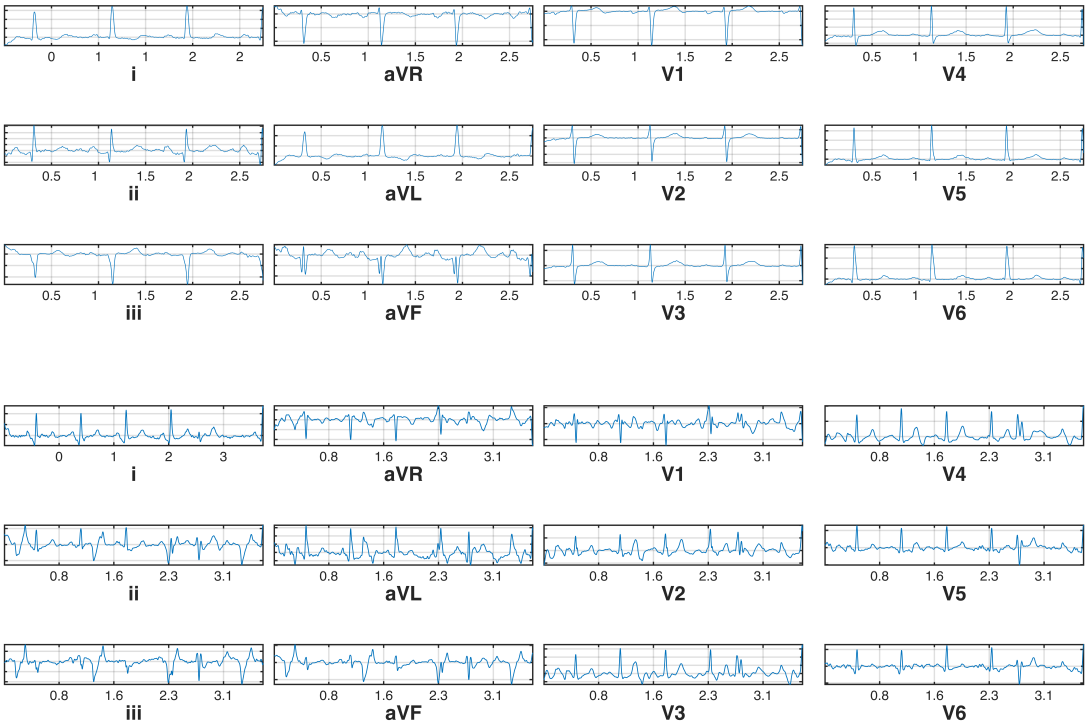

Fig 13. ECG without motion artifacts: (top) healthy and (bottom) non-healthy subjects.

Table 4. Performance of the single model trained to denote all leads.

Leads	True Positive	True Negative	False Positive	False Negative	Accuracy of single model	Accuracy of combined model
I	317	319	1	7	99.38%	99.38%
II	317	318	2	3	99.22%	99.22%
III	313	318	2	7	98.59%	98.59%
aVR	318	320	0	2	99.69%	99.59%
aVF	311	319	1	9	98.44%	98.44%
aVL	308	317	3	12	97.66%	97.66%
V1	316	315	5	4	98.59%	98.59%
V2	319	314	6	1	98.91%	98.91%
V3	319	316	4	1	99.22%	99.22%
V4	320	310	10	0	98.44%	98.44%
V5	319	315	5	1	99.06%	99.06%
V6	319	318	2	1	99.53%	99.53%

The unified model architecture demonstrates significant computational advantages over the lead-specific approach. While the combined model requires only a single load operation before prediction, the 12-model alternative necessitates loading all individual networks prior to inference. Our benchmarking tests revealed a substantial performance difference: the unified model achieved prediction times of 1.60 ± 0.05 seconds (mean $\pm$ SD), compared to 21.67 ± 0.12 seconds for the multi-model approach. These metrics are derived from 100 repeated trials of model loading and evaluation, with timing data collected for each iteration and reported as mean values.

The results shown in Fig. 13 are evaluated by the selected model and confirmed by experienced clinicians. Fig. 14 illustrates an ECG with significant noise even after motion artifacts are removed hampering accurate visual diagnostics. This prediction is clearly made by the trained model within 2 seconds whereas an expert may take approximately 5 seconds for visual interpretations. In this scenario, the complete ECGs

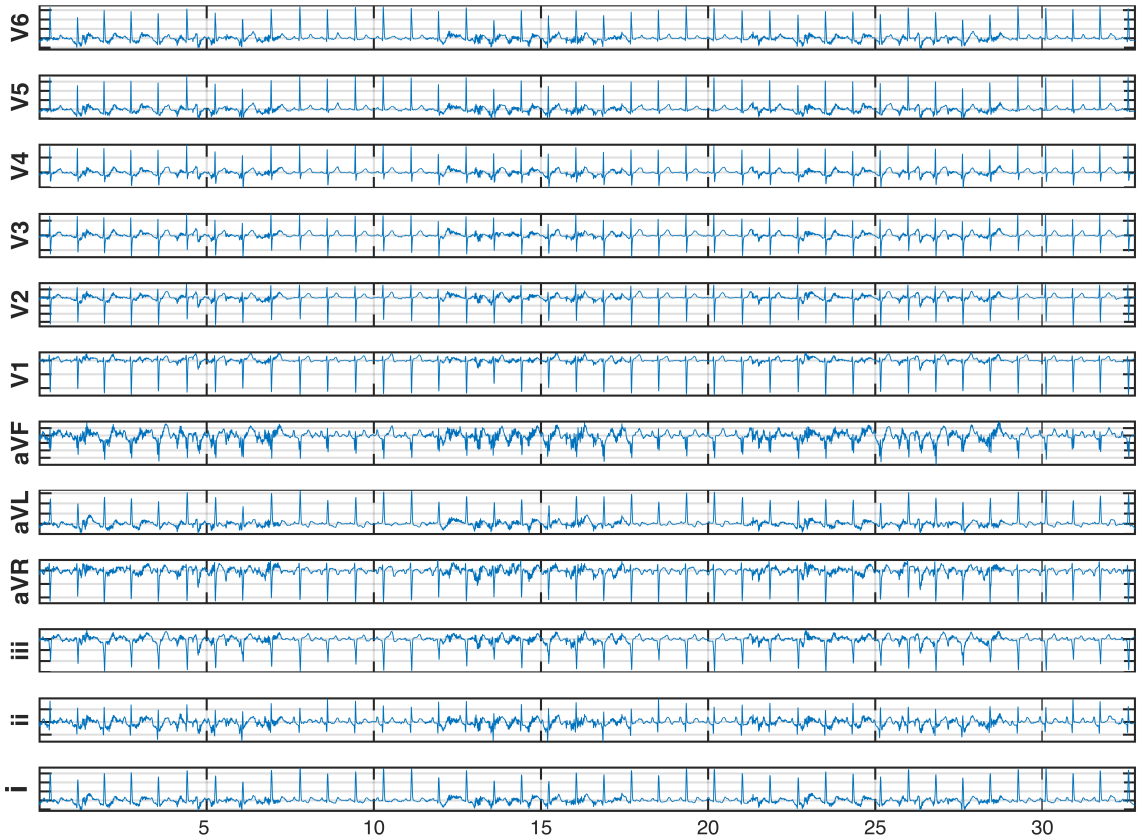

Fig 14. Full ECG found with heavy motion artifacts.

will be produced only if the physician selects the option to generate a full ECG.

1.6 Motion Artifacts Removal

One of the most challenging aspects of this study is to reduce motion artifacts while retaining the correct ECG data that may possibly aid in identifying various underlying medical conditions. For this purpose, the assistance of many cardiographers are obtained to fine-tune application settings to produce an accurate output while ensuring that critical medical interpretation from the original ECG are not excluded.

As seen in Fig. 10, we may unequivocally determine that the *Savitzky-Golay filter* has enhanced the clarity of the ECG output. The MSE, on the other hand, must be computed to see if this filter had actually reduced this error and at the same time, making it more legible.

During the initial stage in eliminating motion artifacts, the M value, which represents the SWT's decomposition level, is chosen to be 5. Initially, this value is chosen as explained in the [36] to obtain a better de-noising effect. Subsequently, after the routine is completed, another test is conducted to determine the SWT's optimal decomposition level as in and Fig. 2. As a consequence, it is recommended to utilize M = 7 for the ECGs in the 1000Hz frequency range. This enabled us to reorganize the software to provide a highly accurate ECG output when motion artifacts are removed. The outcome of each procedure is evaluated by experts in the subject matter to fine-tune the software to provide the most accurate information possible.

1.7 Deep ConvNet for ECG Evaluation

An important task in this research is to determine the optimal number of machine learning models to train the data with. Initially, a single model is assigned for each lead which produced the results as given in Table 3 resulting in more than 95% of accuracy at all times. Next, a model is created using all leads combined or simply saying, a combined model, to evaluate the data which produced more than 97.66% accuracy at all times as shown in Table 4.

These result clearly demonstrate that when all leads are merged together, the combined model outperforms all other models except in Lead III and as such, it is preferable to utilize a mixed model for ECG assessment. The improved accuracy of the combined model may be due to each signal's similarity when compared with one another as these signals only indicate the amount of voltage received by each electrode between the heart beats. As the lag time between the leads is negligible, certain ECG signals are not identical but somewhat comparable in signal strength. Hence, having over 30,000 images with such a resemblance will certainly assist the model in learning about signals and associated noise levels.

The unified model offers significant advantages in resource efficiency compared to training individual lead-specific models. Specifically, it reduces storage requirements by an order of magnitude (1 GB vs. 15 GB for 12 separate models) and accelerates inference time. This performance improvement stems from eliminating redundant operations: while the combined model loads parameters once, the multi-model approach incurs repeated I/O overhead by loading 12 independent H5 files sequentially.

1.8 Novelty, Contribution and Scope

Novelty

This work introduces several novel aspects to the field of ECG motion artifact detection and removal. Unlike previous approaches that focus solely on either artifact removal or quality assessment, this study presents an integrated framework that combines SWT preprocessing with deep CNN-based quality evaluation in a unified pipeline. Rather than training separate models for each of the 12 ECG leads, this work demonstrates that a single combined CNN model can effectively evaluate all leads simultaneously, representing a departure from traditional lead-specific approaches. The study proposes a modified threshold calculation that improves robustness against motion-induced artifacts compared to existing methods, specifically addressing limitations in [28]. Additionally, the research demonstrates significant computational efficiency improvements (1.6 vs. 21.7 seconds) while maintaining high accuracy, making the approach viable for clinical real-time applications.

Contribution

The primary contributions of this research to the biomedical engineering field encompass both technical and clinical advances. From a technical perspective, this work achieves 98.76% classification accuracy in distinguishing between usable and artifact-corrupted ECG signals, with sensitivity of 98.74% and specificity of 98.77%. The study develops a resource-efficient solution that reduces storage requirements from 15GB (12 separate models) to 1GB (unified model) while accelerating inference time by approximately 13-fold. The methodological innovation integrates multi-resolution thresholding with Savitzky-Golay filtering to preserve critical ECG morphological features while effectively removing motion artifacts, supported by comprehensive evaluation using 12-lead ECG data with expert validation. From a clinical standpoint, the enhanced ECG signal quality reduces the risk of misdiagnosis caused by motion

artifacts in resting ECG recordings. The automated quality assessment can reduce clinician workload by providing rapid ($\leq$ 2 seconds) signal evaluation compared to manual interpretation, while offering a systematic approach to artifact detection that could improve consistency in ECG quality assessment across different clinical settings.

Limitations

While this study presents significant advances, several limitations must be acknowledged across technical, methodological and clinical domains. The research relies on publicly available PhysioNet datasets, which may not fully represent the diversity of motion artifacts encountered in real clinical environments with different patient populations, recording conditions and equipment variations. The focus on motion artifacts means the system may not effectively handle other common ECG noise sources such as power line interference, electrode contact issues or electromagnetic interference from medical devices. The optimal decomposition level (M=7) was determined specifically for 1000Hz ECG signals, potentially limiting applicability to systems using different sampling frequencies commonly found in clinical practice, while the study depends on expert visual assessment for ground truth labeling, introducing potential subjectivity and inter-observer variability. The current system has not been extensively tested across a comprehensive range of cardiac pathologies, which may affect its generalizability to diverse patient populations with various heart conditions. The thresholding parameters ($c \in [2, 2.5]$) are empirically determined and may require adjustment for different patient populations or recording conditions. Expert validation was conducted with a limited number of clinicians, requiring broader clinical validation studies to establish inter-rater reliability and clinical utility. The study does not address regulatory approval requirements or clinical validation standards necessary for deployment in healthcare settings, nor does it characterize system performance on borderline cases where artifact presence is ambiguous. Limited evaluation across different patient demographics, body types and clinical conditions that may affect ECG signal characteristics and artifact patterns represents another constraint that future research must address through expanded datasets, multimodal physiological signal incorporation, adaptive parameter selection mechanisms, large-scale clinical validation studies and investigation of real-time integration capabilities with commercial ECG systems.

Conclusion

This study introduces a deep learning–based framework for the detection and removal of motion artifacts in resting ECG signals, aiming to improve diagnostic reliability in clinical settings. By integrating advanced preprocessing methods with a robust classification model, the proposed approach effectively distinguishes between clean and artifact-contaminated signals, thereby enhancing ECG usability for medical decision-making. The results demonstrate notable improvements in clarity and diagnostic quality, indicating that deep learning can serve as a valuable tool in minimizing the risk of misdiagnosis caused by motion-induced noise. Despite these achievements, the current system relies on manually collected ECG datasets and does not encompass all known cardiac disorders, which may limit its generalizability. Future work will focus on integrating the algorithm directly into ECG acquisition devices to enable real-time artifact detection and correction. Additionally, expanding the training dataset to include a broader spectrum of cardiac pathologies will improve robustness and reduce the likelihood of misclassification. Incorporating multimodal physiological signals, such as photoplethysmography (PPG) or accelerometer data, could further enhance the model's artifact detection accuracy. Ultimately, these developments will

advance the reliability, automation and clinical adoption of ECG-based diagnostics.

Data availability statement

The raw image dataset used in this study is publicly available at: https://www.physionet.org. All relevant data supporting the findings of this study are included within the manuscript.

Funding

The authors received no specific funding for this work.

Competing interests

The authors have declared that no competing interests exist.

References

1. Lena Biel, Ola Pettersson, Lennart Philipson, and Peter Wide. ECG analysis: A new approach in human identification. *Instrumentation and Measurement, IEEE Transactions on*, 50:808–812, July 2001. (document)

2. Dirk Durrer. Electrical Aspects of Human Cardiac Activity: A Clinical-Physiological Approach to Excitation and Stimulation†. *Cardiovascular Research*, 2(1):1–18, January 1968. (document)

3. Martijn L. Bakker, Antoon F. M. Moorman, and Vincent M. Christoffels. The atrioventricular node: origin, development, and genetic program. *Trends in Cardiovascular Medicine*, 20(5):164–171, July 2010. (document)

4. David B Geselowitz. On the theory of the electrocardiogram. In *Proceedings of the IEEE*, volume 77, 2002. (document)

5. Amit Kumar and Mandeep Singh. Optimal Selection of Wavelet Function and Decomposition Level for Removal of ECG Signal Artifacts. *Journal of Medical Imaging and Health Informatics*, 5(1):138–146, February 2015. (document)

6. Antonio Lanata et al. A Novel Algorithm for Movement Artifact Removal in ECG Signals Acquired from Wearable Systems Applied to Horses. *Plos 1*, 10(10), 2015. (document)

7. D. A. Tong, K. A. Bartels, and K. S. Honeyager. Adaptive reduction of motion artifact in the electrocardiogram. In *Proceedings of the Second Joint 24th Annual Conference and the Annual Fall Meeting of the Biomedical Engineering Society] [Engineering in Medicine and Biology*, volume 2, pages 1403–1404 vol.2, 2002. 1

8. J. Lee, D. D. McManus, S. Merchant, and K. H. Chon. Automatic Motion and Noise Artifact Detection in Holter ECG Data Using Empirical Mode Decomposition and Statistical Approaches. *IEEE Transactions on Biomedical Engineering*, 59(6):1499–1506, June 2012. 1

9. F. Strasser, M. Muma, and A. M. Zoubir. Motion artifact removal in ECG signals using multi-resolution thresholding. In *2012 Proceedings of the 20th European Signal Processing Conference (EUSIPCO)*, pages 899–903, August 2012. 1, 1, 1.2.2, 1.2.2, 6

10. S. M. Debbal and F. Bereksi-Reguig. Analysis of ECG signal denoising method based on Stransform. *Medical & Biological Engineering & Computing*, 51(9):1037–1046, 2013. 1

11. Gracee Agrawal, Manju Singh, V. R. Singh, and H. R. Singh. Reduction of artifacts in 12-channel ECG signals using FastICA algorithm. *JSIR Vol.67(1) [January 2008]*, January 2008. 1

12. Serkan Kiranyaz, Turker Ince, and Moncef Gabbouj. Real-Time Patient-Specific ECG Classification by 1-D Convolutional Neural Networks. *IEEE transactions on bio-medical engineering*, 63(3):664–675, March 2016. 1

13. Y. Xia, N. W. D. Leung, H. Yang, L. Wang, and X. Chen. A hybrid wavelet-CNN approach for ECG signal denoising. In *2018 IEEE International Conference on Bioinformatics and Biomedicine (BIBM)*, pages 1219–1224, 2018. 1

14. Francisco Castells, Pablo Laguna, Leif Sörnmo, Andreas Bollmann, and José Millet Roig. Principal Component Analysis in ECG Signal Processing. *EURASIP Journal on Advances in Signal Processing*, 2007(1):074580, December 2007. 1

15. Udit Satija, Barathram Ramkumar, and M. Sabarimalai Manikandan. A Review of Signal Processing Techniques for Electrocardiogram Signal Quality Assessment. *IEEE Reviews in Biomedical Engineering*, 11:36–52, 2018. Conference Name: IEEE Reviews in Biomedical Engineering. 1, 1.1.1

16. F. Andreotti, H. Phan, N. Cooray, C. Lo, M. T. M. Hu, and L. De Vos. Deep learning based framework for automatic detection of motion artifacts in ECG signals. *Computing in Cardiology*, 44, 2017. ISSN 2325-887X. 1

17. M. M. A. Rahhal, Y. Bazi, H. AlHichri, N. Alajlan, F. Melgani, and R. R. Yager. Deep learning approach for active classification of electrocardiogram signals. *Information Sciences*, 345:340–354, June 2016. 1

18. A. L. Goldberger, L. A. N. Amaral, L. Glass, J. M. Hausdorff, P. Ch. Ivanov, R. G. Mark, J. E. Mietus, G. B. Moody, C.-K. Peng, and H. E. Stanley. PhysioBank, PhysioToolkit, and PhysioNet: Components of a new research resource for complex physiologic signals. *Circulation*, 101(23):e215–e220, 2000 (June 13). Circulation Electronic Pages: http://circ.ahajournals.org/content/101/23/e215.full PMID:1085218; doi: 10.1161/01.CIR.101.23.e215. 1.1

19. Xiaoran Ning, Ivan W. Selesnick, and Laurent Duval. Chromatogram baseline estimation and denoising using sparsity (BEADS). *Chemometrics and Intelligent Laboratory Systems*, 139:156–167, December 2014. 1.1.1

20. Mashud Khan, Faizan Aslam, Tahir Zaidi, and Shoab A. Khan. Wavelet Based ECG Denoising Using Signal-Noise Residue Method. In *2011 5th International Conference on Bioinformatics and Biomedical Engineering*, pages 1–4, May 2011. ISSN: 2151-7622. 1.1.1

21. Fuad A. Ghaleb, Maznah Bte Kamat, Mazleena Salleh, Mohd Foad Rohani, and Shukor Abd Razak. Two-stage motion artefact reduction algorithm for electrocardiogram using weighted adaptive noise cancelling and recursive Hampel filter. *PLOS ONE*, 13(11):e0207176, November 2018. Publisher: Public Library of Science. 1.2

22. M.J. Shensa. The discrete wavelet transform: wedding the a trous and Mallat algorithms. *IEEE Transactions on Signal Processing*, 40(10):2464–2482, October 1992. 1.2.2

23. G. P. Nason and B. W. Silverman. The Stationary Wavelet Transform and some Statistical Applications. In Anestis Antoniadis and Georges Oppenheim, editors, *Wavelets and Statistics*, Lecture Notes in Statistics, pages 281–299. Springer, New York, NY, 1995. 1.2.2

24. Mohammad Shahbakhti, Maxime Maugeon, Matin Beiramvand, and Vaidotas Marozas. Low Complexity Automatic Stationary Wavelet Transform for Elimination of Eye Blinks from EEG. *Brain Sciences*, 9(12):352, December 2019. 1.2.2

25. S. G. Mallat. A theory for multiresolution signal decomposition: the wavelet representation. *IEEE Transactions on Pattern Analysis and Machine Intelligence*, 11(7):674–693, July 1989. 1.2.2, 2

26. Harender and R. K. Sharma. EEG signal denoising based on wavelet transform. In *2017 International conference of Electronics, Communication and Aerospace Technology (ICECA)*, pages 758–761, Coimbatore, April 2017. IEEE. 2

27. David L. Donoho and Jain M. Johnstone. Ideal spatial adaptation by wavelet shrinkage. *Biometrika*, 81(3):425–455, September 1994. 1.2.2

28. Szi-Wen Chen, Hsiao-Chen Chen, and Hsiao-Lung Chan. A real-time QRS detection method based on moving-averaging incorporating with wavelet denoising. *Computer Methods and Programs in Biomedicine*, 82(3):187–195, June 2006. 1.2.2, 3, 4, 1.2.2, 1.2.2, 1.8

29. Lisa Torrey and Jude Shavlik. Transfer Learning, 2010. ISBN: 9781605667669 Pages: 242-264 Publisher: IGI Global. 1.3.2

30. Karen Simonyan and Andrew Zisserman. Very Deep Convolutional Networks for Large-Scale Image Recognition. *arXiv:1409.1556 [cs]*, September 2014. arXiv: 1409.1556. 1.3.2, 1.3.3

31. Muhammad Mateen, Junhao Wen, Nasrullah, Sun Song, and Zhouping Huang. Fundus Image Classification Using VGG-19 Architecture with PCA and SVD. *Symmetry*, 11(1):1, January 2019. Number: 1 Publisher: Multidisciplinary Digital Publishing Institute. 1.3.2

32. Hengjin Ke, Dan Chen, Xiaoli Li, Yunbo Tang, Tejal Shah, and Rajiv Ranjan. Towards Brain Big Data Classification: Epileptic EEG Identification With a Lightweight VGGNet on Global MIC. *IEEE Access*, 6:14722–14733, 2018. Conference Name: IEEE Access. 1.3.2

33. Alex Krizhevsky, Ilya Sutskever, and Geoffrey E Hinton. ImageNet Classification with Deep Convolutional Neural Networks. In *Advances in Neural Information Processing Systems*, volume 25. Curran Associates, Inc., 2012. 1.3.3

34. Kaiming He, Xiangyu Zhang, Shaoqing Ren, and Jian Sun. Deep Residual Learning for Image Recognition. *arXiv:1512.03385 [cs]*, December 2015. arXiv: 1512.03385. 1.3.3

35. Abraham Savitzky and Marcel J. E. Golay. Smoothing and differentiation of data by simplified least squares procedures. *Analytical Chemistry*, 36(8):1627–1639, 1964. 1.4

36. Suyi Li and Jun Lin. The Optimal De-noising Algorithm for ECG Using Stationary Wavelet Transform. In *2009 WRI World Congress on Computer Science and Information Engineering*, volume 6, pages 469–473, March 2009. 1.6